Fusion, direct, and total reaction cross sections of the $^{10}B + ^{14}N$ system up to $E_{^{14}N} = 180$ MeV

M. E. Ortiz,* J. Gomez del Campo, Y. D. Chan,† D. E. DiGregorio,‡
J. L. C. Ford, and D. Shapira
Oak Ridge National Laboratory, Oak Ridge, Tennessee 37830

R. G. Stokstad
Lawrence Berkeley Laboratory, Berkeley, California 94720

J. P. F. Sellschop
Witwatersrand University, Johannesburg, South Africa

R. L. Parks
University of Virginia, Charlottesville, Virginia 22901

D. Weiser
Australian National University, Canberra, Australia
(Received 5 October 1981)

The fusion cross section of the $^{10}B + ^{14}N$ system has been measured at five energies covering the range $E_{^{14}N} = 86-180$ MeV. Angular distributions of fusion and direct reaction components for products from $Z = 3$ to $Z = 11$ have been determined. Hauser-Feshbach calculations of the Z distributions, energies and angular distributions of the evaporation residues are presented and compared to the data. The fusion cross section decreases slowly with increasing energy and reaches a maximum angular momentum of about $21 \pm 1\hbar$. The fusion cross section is discussed in terms of entrance channel models and compound nucleus formation and is compared to that of the $^{12}C + ^{12}C$ system. The experimental total reaction cross sections are in good agreement with optical model calculations with parameters deduced from elastic scattering.

[NUCLEAR REACTIONS $^{14}N + ^{10}B$, $E_{^{14}N} = 86$ to 180 MeV, measured $d^2\sigma/d\Omega\, dE$ for reaction products from $Z = 3$ to 11. Extracted σ_{fusion}, σ_{direct}, and σ_{total}.]

I. INTRODUCTION

Many fusion measurements have been carried out for compound nuclei in the mass region $A = 24-40$,[1-9] but it is still uncertain whether the fusion cross section is limited by the dynamical properties of the entrance channel or by the yrast line of the compound nucleus. The $^{14}N + ^{10}B$ system has been chosen in order to study these effects because it forms the same ^{24}Mg compound nucleus as does $^{12}C + ^{12}C$ for which data are available for comparison.[4,5,10,11] Although it has been shown[9] that for $E_{c.m} > 30$ MeV, the method of extracting the fusion cross section σ_{fus} becomes difficult due to the presence of strong noncompound-nucleus components, the separation of the direct reaction products from those of fusion has been made by simple kinematical arguments.[9] Here, we present a description of the data and analyses of the fusion and direct reaction components and the elastic scattering. The analysis of the latter yields σ_R, the total reaction cross section which may be compared directly with the sum of the fusion and direct reaction components. The experimental procedure and the results are described in Sec. II. Analysis of the evaporation residues, the Hauser-Feshbach Monte Carlo calculation, and its comparison to the data are discussed in Sec. III. The direct reaction cross

section and optical model analysis of the elastic scattering are described in Sec. IV. In Sec. V the fusion cross section is discussed and compared with that of the $^{12}C + {}^{12}C$ system.

II. EXPERIMENT AND RESULTS

Beams of ^{14}N at energies of 86.0, 103.8, 149.3, 161.3, and 180.0 MeV extracted from the Oak Ridge Isochronous Cyclotron (ORIC) were used to bombard self-supported enriched (98 percent) ^{10}B targets. The thicknesses of the targets (214 and 72 $\mu g/cm^2$) were determined by measuring the energy loss of α particles in the foils and by Rutherford scattering of ^{14}N at 18 MeV. The principal contaminants were 3 percent copper and 5 percent oxygen impurities in the heavier target and an 8 percent oxygen impurity in the lighter target. The appropriate corrections were taken into account in our analyses.

The reaction products were detected with a counter telescope,[12] which measured residual energy (E) in a position sensitive solid state detector and energy loss (ΔE) in an ionization chamber. The detector simultaneously observed five angles in $\sim$1.5-degree (lab) steps. In a later experiment, a similar detector having nine slits one degree (lab) apart, and two solid state ΔE-E telescopes to observe particles at small scattering angles (4 and 9 degrees) were used. The thicknesses of the solid state counters were $\Delta E = 10$ μm and $E = 2000$ μm. Angular distributions were measured from 4 to 38 degrees. The absolute normalization for the cross sections was derived from the target thickness, solid angle, and integrated beam currents. The estimated uncertainty of the measured cross sections was ± 8 percent. In Fig. 1 a typical two-dimensional E-ΔE spectrum measured at $E_{^{14}N} = 149.3$ MeV and a laboratory angle of 11.3 degrees is shown. Elements with $Z = 3$ to $Z = 12$ are adequately resolved. The events for isotopes of $Z \geq 12$ (seen in Fig.1) correspond to the fusion of $^{14}N + {}^{16}O$ due to oxygen contaminant in the target. Energy distributions ($d^2\sigma/d\Omega\, dE$) and energy integrated angular distributions for evaporation residues ($d\sigma/d\Omega$) for each atomic number and for the five ^{14}N energies were extracted from the two-dimensional spectra.

Figure 2 shows typical energy distributions for $Z = 6$, 7, and 8 at 86.0 [Fig. 2(a)] and 180.0 MeV [Fig. 2(b)] which exhibit the basic features of the reaction mechanism. The dashed curves show the unfolding of the fusion component from the yields due to direct processes. The centroids of the lower ener-

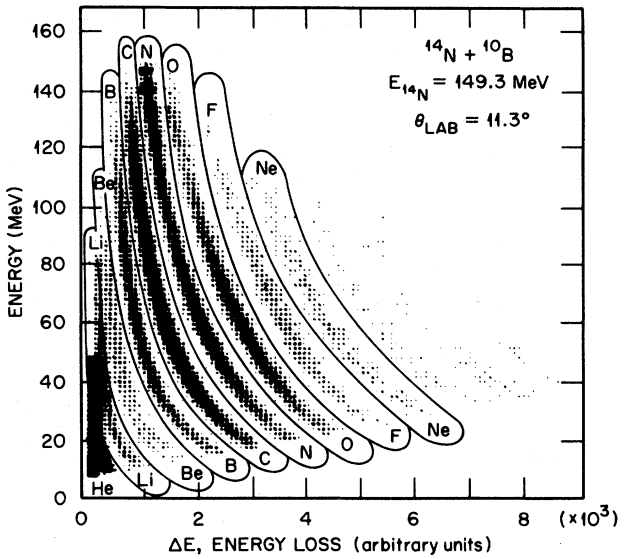

FIG. 1. ΔE vs E array for the reaction products of $^{14}N + {}^{10}B$ at $E_{^{14}N} = 149$ MeV and $\theta_{lab} = 11.3°$. The total energy E was obtained by analog summation of the signals from the ionization chamber and solid-state detector. The curves around the contours of constant Z were used to obtain the projections along the E axis.

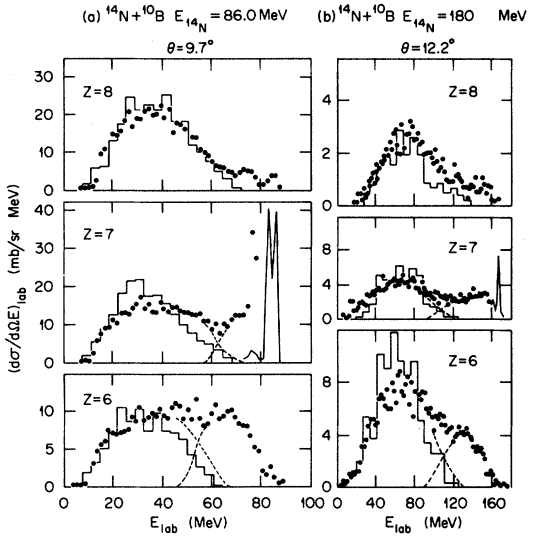

FIG. 2. (a) Energy spectra of oxygen, nitrogen, and carbon ions produced in the $^{14}N + {}^{10}B$ reaction at $E_{^{14}N} = 86$ MeV and $\theta_{lab} = 9.7°$. The histograms are the results of Monte Carlo calculations discussed in the text. The dashed lines for the nitrogen and carbon spectra indicate separation assumed between low-energy (evaporation residues) and high-energy (direct reaction products) components. (b) Energy spectra of oxygen, nitrogen, and carbon ions from the $^{14}N + {}^{10}B$ reaction at $E_{^{14}N} = 180$ MeV and $\theta_{lab} = 12.2°$. The curves through the data points have the same meaning as in (a).

gy groups in these distributions all occur at approximately the energy corresponding to the velocity of the compound nucleus. The higher energy components, whose velocities are close to that of the projectile, arise from direct reaction processes.

The corresponding angular distributions of the evaporation residues are plotted Fig. 3. As an example illustrating the difference between the angular distributions of the evaporation residues and the direct reaction products, Fig. 4 shows angular distributions of the direct reaction components at 180 MeV which are to be compared with those shown in Fig. 3. Note that, while the angular distributions appearing in Fig. 4 are strongly forward peaked, the evaporation residue distributions in Fig. 3 shift toward larger angles as more mass is evaporated.

The evaporation residue cross sections were extracted for all energies by integrating their angular distributions. The contribution resulting from extrapolating the angular distributions over unmeasured angles is less than 10 percent. The results for the evaporation residue cross sections at the five energies are summarized in Table I. Columns 1 to 10 give the bombarding energy E_{lab}, the center-of-mass energy $E_{\text{c.m.}}$, the excitation energy in the compound nucleus E_x, and the evaporation residue cross section σ_{ER} for each atomic number Z. The major source of errors arises from uncertainties in the solid angle, target thickness, beam current integration, and oxygen contamination (important only for $Z \geq 9$). The direct reaction cross sections were obtained by integration of the angular distributions such as those shown in Fig. 4, and the results for each atomic number Z are given in Table II. Angular distributions for the elastic scattering were also measured at 1-degree intervals and with an angular resolution of about 0.8 degrees. The experimental angular distribution for $E_{^{14}\text{N}} = 86$ MeV is plotted in Fig. 5, together with the optical model fit.

III. ANALYSIS OF THE EVAPORATION RESIDUES

The experimental yields and the energy and angular distributions of the evaporation residues were compared with statistical model predictions using the Monte Carlo evaporation code LILITA.[13] The Monte Carlo calculations are described in detail in Ref. 9; the same set of parameters was used for the calculations in this work. The calculations of the energy spectra and angular distributions, however, were done using quantum mechanical angular distributions for the emission of the light particles (see

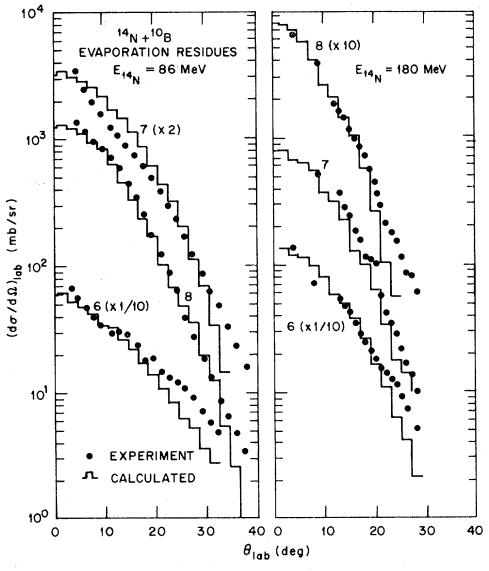

FIG. 3. Angular distributions of evaporation residues of oxygen, nitrogen, and carbon at $E_{^{14}\text{N}} = 86$ MeV (left side) and 180 MeV (right side) for the $^{14}\text{N} + ^{10}\text{B}$ fusion reaction. The data are the experimental cross sections and the histograms are the Monte Carlo calculations discussed in the text.

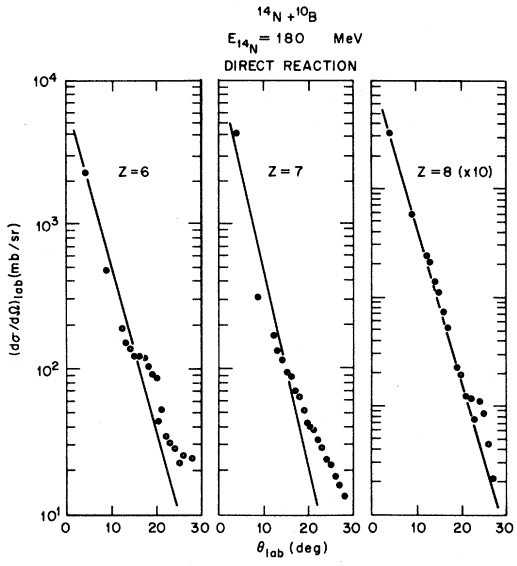

FIG. 4. Angular distributions of the direct reaction products for the $^{14}\text{N} + ^{10}\text{B}$ system at $E_{^{14}\text{N}} = 180$ MeV. The solid line is the result of the diffraction model analysis discussed in the text.

TABLE I. Evaporation residue cross sections measured at five bombarding energies for the $^{14}N + {}^{10}B$ system.

E_{lab} (MeV)	$E_{c.m.}$ (MeV)	E_x (MeV)	σ_{ER} (mb) $Z=5$	$Z=6$	$Z=7$	$Z=8$	$Z=9$	$Z=10$	$Z=11$
86.0	35.83	64.68	51	186	300	241	107	77	9.5
103.8	43.75	72.1	94	252	233	238	67	40	7.1
149.0	62.08	91.05	130	291	175	173	36	14	3.3
161.3	67.21	96.06	136	280	205	98	20	5	1.4
180.0	73.51	104.16	104	250	145	86	13	3	0.4

Ref. 13), rather than using the Ericson-Strutinski approach which was used in the calculations shown in Ref. 9. The Monte Carlo Hauser-Feshbach calculations (histograms) and the experimental energy distributions for carbon, nitrogen, and oxygen at the extreme ^{14}N energies (86 and 180 MeV) are included in Fig. 2. The agreement with the data shown here suggests that the fusion cross sections can be extracted for residues with Z values comparable to or even less than that of the projectile. As the Z of the residue decreases, the average energy decreases and the width of the distribution increases; this feature is consistent with the calculations, which further supports our technique for unfolding the spectra because the centroids of the distributions of the extracted evaporation residues all occur at an energy which corresponds approximately to the velocity of the compound nucleus.

The calculated angular distributions given in Fig. 3 show good agreement with the data. In Fig. 6, angle integrated yields for evaporation residues from $Z=5$ to 11 are compared to the Hauser-Feshbach calculations (solid lines) for bombarding energies from 80 to 180 MeV. These yields are plotted as percentages of the total fusion cross sections. The general trend of the data with bombarding energy is well reproduced by the calculations, although some discrepancies are seen for $Z=8$, 7, and 5 at the lowest bombarding energies. Such deviations may arise from the use of the sharp cutoff approximation for the transmission coefficients as

TABLE II. Experimental direct reaction cross sections for the $^{14}N + {}^{10}B$ system.

	E_{lab} (MeV)				
Z	86.0	103.8	149.3	161.3	180.0
3	27	85	124	142	174
4	14	42	62	60	48
5	14	29	26	50	72
6	48	97	108	129	189
7	81	86	83	83	85
8		21	35	38	23
σ_{DI}(mb)	184±18	360±36	438±44	502±50	591±60

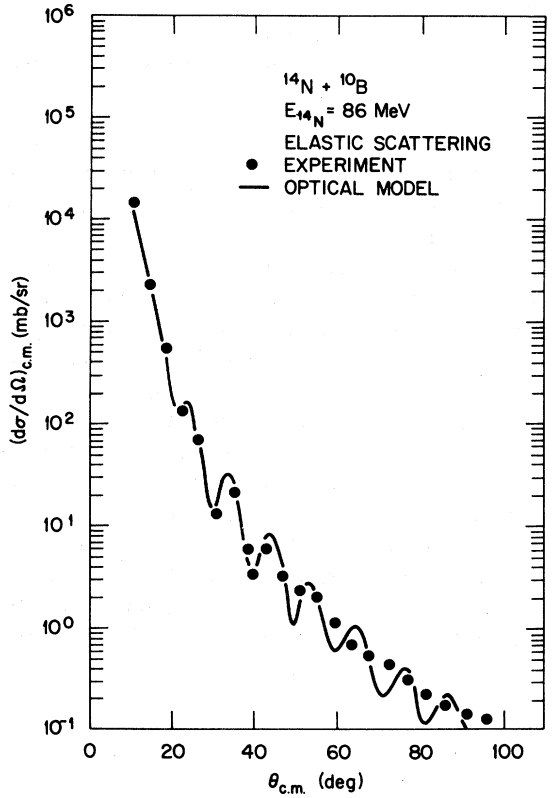

FIG. 5. The elastic scattering angular distributions for the $^{14}N + {}^{10}B$ system at $E_{^{14}N}=86$ MeV. The optical model fit is given by the solid curve and the parameters are given in Table III.

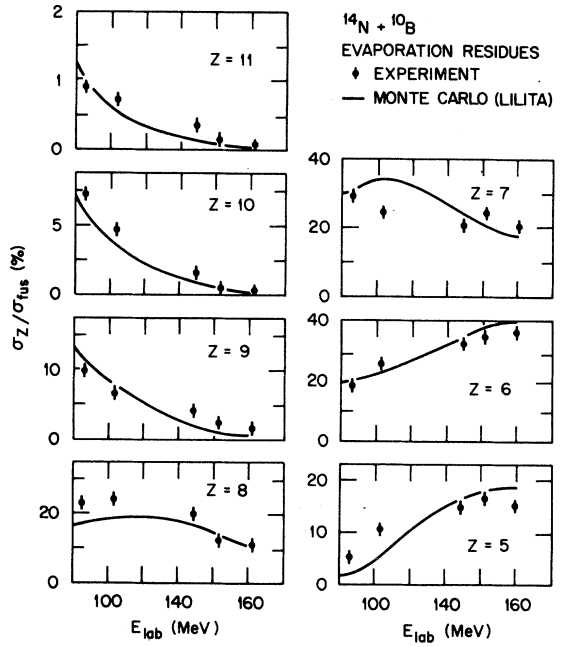

FIG. 6. Total yields of evaporation residues for the $^{14}N + ^{10}B$ fusion reaction. The ordinate gives the amount of evaporation residue cross section for a given Z value as a percent of σ_{fus}, and the horizontal scale gives the ^{14}N bombarding energy. The Hauser-Feshbach calculations are given by the solid line.

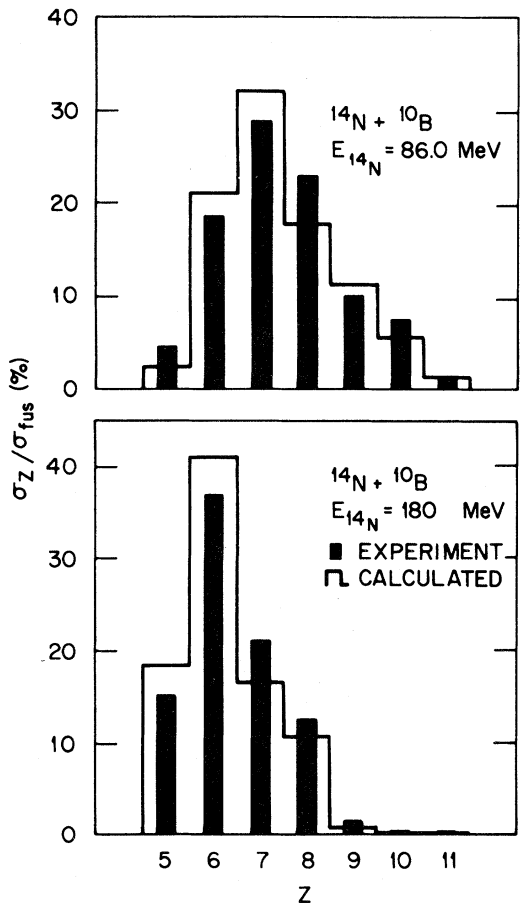

FIG. 7. Yields of evaporation residues, given as a percent of σ_{fus} measured for the two extreme bombarding energies 86 and 180 MeV. The solid bars represent the experimental measurements and the histogram the results of the Monte Carlo calculations.

well as from uncertainties in parametrizing the Fermi gas model at low densities (for nuclei of low mass number).

The residue yields are plotted as percentages of the total fusion cross versus Z for the two extreme bombarding energies of 86 and 180 MeV in Fig. 7. The corresponding Monte Carlo Hauser-Feshbach results are represented by the histograms. As can be seen, the maxima and dispersion of the Z distributions are quite well reproduced, which is a further indication that the residues are consistent with the decay of an equilibrated compound nucleus. The overall agreement of the energy, angular, and Z distributions of the data with the calculations indicates the absence of significant two-body contributions with large negative Q values to the yields taken as evaporation residues.

IV. DIRECT REACTION CROSS SECTIONS

The total reaction cross section σ_R is defined by $\sigma_R = \sigma_{fus} + \sigma_{DI}$, where σ_{DI} is the direct reaction cross section. These components were extracted by the deconvolution procedures illustrated in Fig. 2, where the dashed lines separate the direct reaction and the evaporation residue components. In Fig. 2, at high ejectile energies, the energy spectra show sharp energy groups corresponding to the excitation of single states or clusters of states in the residual nuclei populated by transfer and inelastic scattering reactions. In addition, however, one can see the presence of continuous distributions, particularly prominent in $Z=7$ and $Z=6$, centered around $E \simeq 70$ MeV for $E_{^{14}N}=86$ MeV [Fig. 2(a)] and around $E=130$ MeV for $E_{^{14}N}=180$ MeV [Fig. 2(b)]. These continuous distributions can be associated with a peripheral process such as projectile fragmentation and are very similar to the continuous spectra seen when light projectiles (^{16}O,^{14}N) are incident on heavy targets.[14] In a recent analysis of the $^{14}N + ^{12}C$ reaction[15] it is also shown that these

continuous energy distributions can be associated with the direct excitation of the projectile followed by particle emission. This seems to be the case also for $^{16}O + ^{12}C$ peripheral reactions studied by Rae *et al.*[16] at $E_{^{16}O} = 145$ MeV. These peripheral processes are considered as part of the direct reaction cross sections and thus are incorporated into σ_{DI}. At very forward angles these continuous distributions dominate the differential cross sections. Figure 8 shows the energy spectra of boron and carbon isotopes measured at $\theta_{lab} = 3.8$ degrees. The histograms are the expected yields for the evaporation residue portion as calculated with the code LILITA[13] and the dashed lines indicate the separation between direct and evaporation components.

The angular distributions shown in Fig. 4 were obtained by adding these continuous and discrete components of the high energy portion of the spectra. The contribution of the low energy recoiling partners to the direct reaction yield are assumed to be negligible, since they occur at angles larger than 30 degrees for most of the relevant range of reaction Q values. Following the analysis of Ref. 9 for the $^{14}N + ^{12}C$ reaction, one may use a simple diffraction model to interpret the slope of the angular distributions of Fig. 4. The relevant relations[17] are

$$\frac{d\sigma}{d\Omega} \propto \frac{\theta_{c.m.}}{\sinh^2(\pi\Delta\theta_{c.m.})} \tag{1}$$

for the inelastic channels, and

$$\frac{d\sigma}{d\Omega} \propto \frac{1}{\theta_{c.m.}\sinh^2(\pi\Delta\theta_{c.m.})} \tag{2}$$

for the elastic channel. In Eqs. (1) and (2), $\theta_{c.m.}$ is the center-of-mass scattering angle and Δ is related to the modulus of the scattering matrix elements

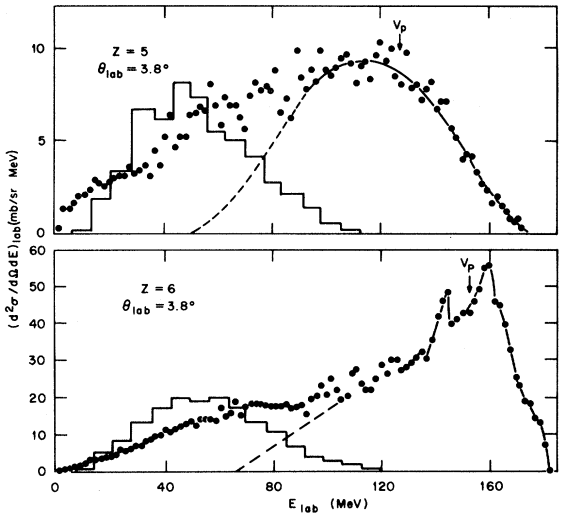

FIG. 8. Energy spectra for carbon and boron isotopes from the $^{14}N + ^{10}B$ reaction at $E_{^{14}N} = 180$ MeV and $\theta_{lab} = 3.8°$. The dashed lines indicate the separation between the high (direct) and low (evaporation residue) energy components. The histograms are predictions of the Monte Carlo Hauser-Feshbach calculations.

$|S_l|$ by

$$|S_l| = \frac{1}{1+\exp|(L-l)/\Delta|} . \tag{3}$$

The values of the $|S_l|$ were determined by fitting the elastic scattering at each energy with the optical model parameters of Table III, and the values of L are determined from the scattering matrix elements by the condition $|S_l| = 0.5$. With these parametrizations the deduced value of Δ ranged from 0.9 at 86 MeV to 1.5 at 180 MeV.

The solid lines of Fig. 4 are the result of such dif-

TABLE III. Total reaction cross sections and optical model parameters for the $^{14}N + ^{10}B$ system. The real part was fixed for all energies to be $V = 23.614$ MeV, $r_0 = 1.25$ fm, and $a_0 = 0.52$ fm. The geometry of the imaginary potential was taken to be $r_0' = 1.22$ fm and $a_0' = 0.54$ fm. The Coulomb radius r_C was 1.3 fm.

E_{lab} (MeV)	$E_{c.m.}$ (MeV)	W (MeV)	σ_R^{op} (mb)	σ_R (exp) (mb)
86.0	35.83	11.354	1308	1229±100
103.8	43.75	14.699	1356	1356±108
149.3	62.08	15.089	1360	1298±103
161.3	67.21	16.954	1375	1295±103
180.0	73.51	17.255	1379	1272±101

fraction model calculations for the inelastic channels. The results for the elastic scattering, using Eq. (2), are shown in Fig. 9. As can be seen, the general agreement between the calculations and the data in Fig. 4 is an indication that the basic mechanism producing these high energy yields is that of direct reactions.

By integrating the direct reaction angular distributions, such as those shown in Fig. 4, the values of $\sigma_{\rm DI}$ were extracted for all bombarding energies and for $Z \leq 8$. The results are given in Table II. The cross sections for $Z=3$ and 4 given in this table are the direct reaction estimates deduced from the total experimental Li and Be by subtracting the predictions of the code LILITA from evaporation residues with $Z=3$ and 4 (these predictions range from 24 mb at $E_{^{14}N}=86$ MeV to 63 mb at $E_{^{14}N}=180.0$ MeV). As pointed out in Ref. 9, the yields of Li and Be expected from evaporation of these nuclei by the compound nucleus may be a significant contribution. However, for the present case of ^{24}Mg, compound nucleus calculations for the first chance evaporation of Li and Be with the code HELGA[18] at $E_{^{14}N}=86$ MeV predicted a total emission of only 5 mb and this process, therefore, was neglected at all energies.

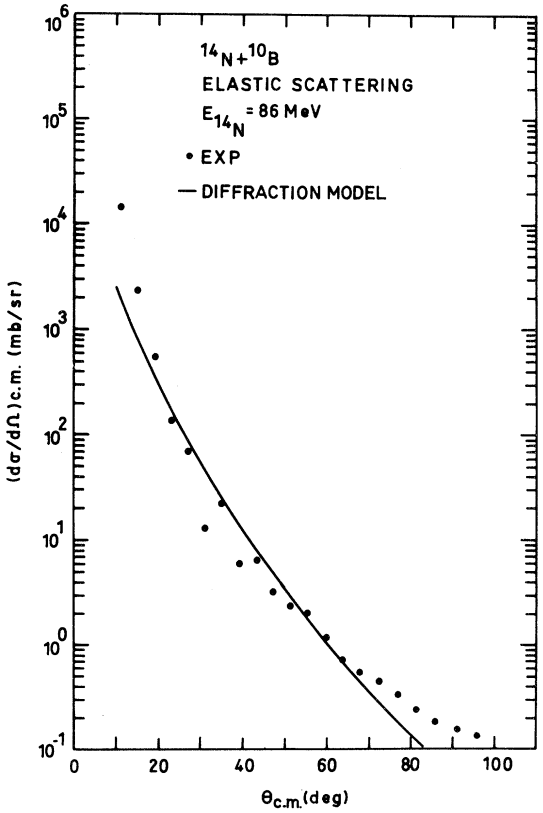

FIG. 9. The elastic scattering of ^{14}N + ^{10}B at $E_{^{14}N}=86$ MeV. The solid line is the angular distribution predicted by the diffraction model.

The total reaction cross sections deduced from the measurements of $\sigma_{\rm fus}$ and $\sigma_{\rm DI}$ are given in Table III; the reaction cross section $\sigma_R^{\rm op}$ was calculated from the optical model fits to the elastic scattering measured at the five bombarding energies given in Table III. The parameters used in the fits are also given in Table III.

V. DISCUSSION OF THE FUSION DATA AND COMPARISON TO ^{12}C + ^{12}C DATA

The fusion cross sections obtained from the evaporation residues are given in Table IV for the five bombarding energies studied. The cross sections for $Z \leq 4$ that were included in the fusion cross sections were 74, 65, 38, 48, and 80 mb for the $E_{^{14}N}$ bombarding energies of 86, 103.8, 149, 161.3, and 180 MeV, respectively. In Fig. 10 the fusion cross section is plotted versus $1/E_{\rm c.m.}$ for the ^{14}N + ^{10}B system. The solid dots correspond to our present measurements and the open circles are those of Ref. 11. The dashed line is the Glas-Mosel prediction with the parameters $r_{\rm cr}=1.17$ fm, $V_{\rm cr}=-1.9$ MeV, $r_B=1.50$ fm, $V_B=6.80$ MeV, and $\hbar\omega=2$ MeV. These parameters are very similar to those for the ^{14}N + ^{12}C system (Ref. 9), except for the critical radius $r_{\rm cr}$ which is 6 percent larger for the ^{10}B + ^{14}N case. Nevertheless, the similarities in the Glas-Mosel parameters would indicate that the fusion of ^{14}N + ^{12}C and ^{14}N + ^{10}B is governed by macroscopic features, i.e., by bulk properties varying as Z and $A^{1/3}$.

At the three highest energies the drop in the fusion cross section is proportional to $1/E_{\rm c.m.}$, as is indicated by the solid line in Fig. 10. This drop is similar to that seen for the ^{10}B + ^{16}O and ^{14}N + ^{12}C

TABLE IV. Experimental fusion cross sections for the ^{14}N + ^{10}B system.

$E_{\rm lab}$ (MeV)	$E_{\rm c.m.}$ (MeV)	$\sigma_{\rm fus}$ (mb)
86.0	35.83	1045±85
103.8	43.75	996±85
149.0	67.08	860±68
161.3	67.21	793±65
180.75	73.51	681±68

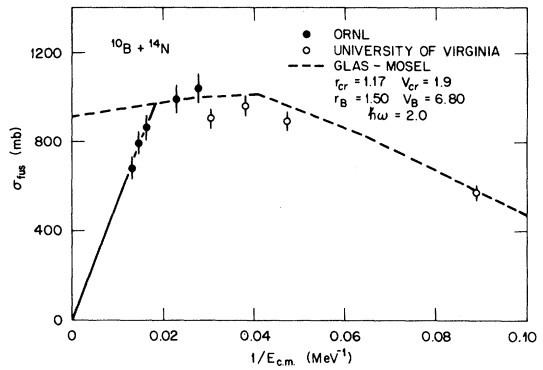

FIG. 10. The fusion cross section (in mb) plotted against $1/E_{\text{c.m.}}$. The solid points are the present results; the open circles are from Ref. 11. The dashed line is the Glas-Mosel fit with the indicated parameters. The solid line intersecting the origin indicates that $\sigma_{\text{fus}} \propto 1/E_{\text{c.m.}}$ at high energies, which can be interpreted as evidence for a saturation of the angular momentum at $21 \pm 1\hbar$.

systems[7] and can be interpreted as due to an absolute angular momentum limit or rotating liquid drop limit (RLD).[19] In the present case, the limiting angular momentum estimated from the fusion data of Fig. 10 is $J_{\max} \simeq 21 \pm 1\hbar$, which is about three units lower than predicted for $A = 24$ according to the RLD calculation of Ref. 19.

The fusion cross section can also be interpreted in terms of possible angular momentum limitations for forming the compound nucleus. In this case, one deduces from the data the critical angular momentum, J_c, given by:

$$\sigma_{\text{fus}} = \frac{\pi\lambda\!\!\!^{-2}}{(2I+1)(2i+1)} \sum_{J}^{J_c} (2J+1) \sum_{s,l} T_{l,s}^{J} , \quad (4)$$

where s, the channel spin, runs from $|I-i|$ to $I+i$. For sufficiently high values of J_c and small channel spins, the use of the sharp cutoff approximation yields the familiar expression

$$\sigma_{\text{fus}} = \pi\lambda\!\!\!^{-2}(J_c+1)^2 . \quad (5)$$

However, for the present case, the channel spin s runs from 2 to 4, and Eq. (5) is a good approximation of Eq. (4) only if the grazing angular momentum l_g is $> J_c + 4$ or if $E_{\text{c.m.}} > 30$ MeV. For this fusion data and that of Ref. 11 we have used Eq. (4) with the sharp cutoff approximation, extending the summation up to l_g, in order to deduce the values of J_c given in Table V. The values of the grazing partial wave l_g were extracted from the optical model calculations and are also given in Table V. For the low J_c values, the difference between the values given in Table V and those deduced from Eq. (5) are as high as $1\hbar$, but for $J_c > 18\hbar$ the difference is only 1 to 2 percent.

Data for the fusion of $^{12}C + ^{12}C$ is available for comparison with the $^{10}B + ^{14}N$ system; this comparison is made in Fig. 11. The solid circles are our measurements (see Table V) for the $^{10}B + ^{14}N$ systems. The open circles are the J_c values obtained from the measurements of Ref. 11 and are also given in Table V. The solid triangles are the results of the $^{12}C + ^{12}C$ fusion measurements by the ANL group.[20] The open triangles and solid squares are also measurements for $^{12}C + ^{12}C$ from Refs. 10 and 11, respectively. The solid lines drawn through the data points are the results of the Glas-Mosel calculations discussed in connection with Fig. 10. These calculations use the same reduced parameters for both systems, $^{12}C + ^{12}C$ and $^{10}B + ^{14}N$. Since

TABLE V. Critical angular momenta for J_c (fusion) for the $^{14}N + ^{10}B$ system.

E_x (MeV)	σ_{fus} (mb)	J_c ($\hbar$)[b]	l_g ($\hbar$)[c]
40.0	576±25[a]	7.5±0.2	8
50.0	896±40[a]	12.5±0.3	14
55.0	961±40[a]	14.4±0.3	16
60.0	903±40[a]	15.0±0.3	18
64.68	1045±85	17.5±0.7	20
72.1	996±85	18.9±0.7	21
91.05	860±68	20.9±0.7	26
96.06	793±65	20.9±0.8	27
104.16	681±68	20.5±1.0	29

[a]Data from Ref. 11.
[b]J_c calculated from Eq. (4).
[c]Grazing angular momentum l_g computed from the optical model fits to the elastic scattering.

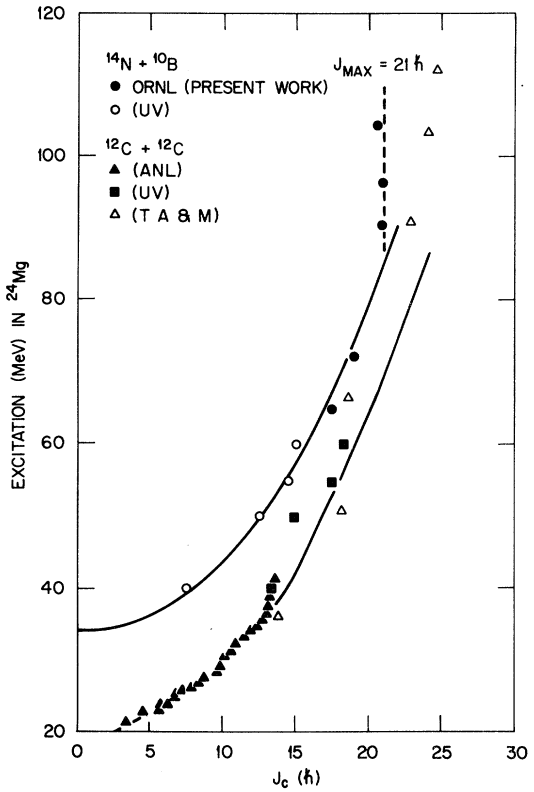

FIG. 11. Comparison of the critical angular momentum J_c vs excitation energy in ^{24}Mg for the $^{14}N + ^{10}B$ and $^{12}C + ^{12}C$ systems. The solid lines are the results of Glas-Mosel calculations using the same set of parameters for both systems.

predicted values of J_c are nearly the same for each system at the same center-of-mass energy, the curves in Fig. 11 are displaced by the difference in separation energies Q_{cn} for the two modes of formation of the compound nucleus.

The absolute error bars in the data points of Fig. 11 have been omitted (although they are typically $\pm 1\hbar$) to emphasize the relative uncertainties which are more important in determining the trend of E_x vs J_c. Although the $^{12}C + ^{12}C$ data show large discrepancies between the various experimental measurements, still they indicate that the general trend is that of the entrance channel limitation since they follow the Glas-Mosel prediction using the same parameters as for the $^{14}N + ^{10}B$ calculation. The data for both systems appear parallel to each other, which indicates that the limitation is in the entrance channel since interpretations based on limitations imposed by the compound nucleus, such as that due to a statistical yrast line (Refs. 21 and 22), would require the overlap of the two fusion bands. Calculations of the statistical yrast line for ^{24}Mg have been given by Vandenbosch,[23] who suggests that the oscillating behavior of the fusion cross section could be due to an yrast limitation. From the present measurements we conclude that the statistical yrast line cannot be the limiting factor for the fusion of $^{10}B + ^{14}N$, although it still is possible that it is the limitation for $^{12}C + ^{12}C$. Therefore, the comparisons in Fig. 11 indicate that the limitation on the fusion of $^{10}B + ^{14}N$ is in the entrance channel since the compound nucleus has states of higher angular momentum available, as shown by the fusion of $^{12}C + ^{12}C$.

One factor that may be responsible for the behavior seen in Fig. 11 is the large difference in separation energy or compound nucleus Q value (Q_{cn}) between the two channels: $Q_{cn} = 28.8$ MeV for $^{10}B + ^{14}N$ and $Q_{cn} = 13.9$ MeV for $^{12}C + ^{12}C$. If $^{10}B + ^{14}N$ reaches the same angular momentum of $\sim 22\hbar$ as does $^{12}C + ^{12}C$ at $E_x = 72$ MeV (see Fig. 11), then the magnitude of the fusion cross section would be 1371 mb which equals the total reaction cross section. The model suggested by Lee *et al.*[21] would also predict a large fusion cross section for $^{10}B + ^{14}N$ in order to have the same statistical yrast line limitation as $^{12}C + ^{12}C$.

For the highest energies there is a pronounced difference between $^{14}N + ^{10}B$ and $^{12}C + ^{12}C$, since the former system indicates a saturation of J_c and the latter does not. This behavior is also quite different from that seen in the $^{16}O + ^{10}B$ and $^{14}N + ^{12}C$ systems, where both show saturation of the angular momentum at $J_c \simeq 26\hbar$.[7] Owing to the large relative errors of the $^{12}C + ^{12}C$ measurements, we believe it is important to improve the accuracy of these measurements as well as to perform an analysis similar to that for $^{14}N + ^{10}B$ in order to confirm the above observation.

It should be emphasized that the experimental total reaction cross section discussed in Sec. IV increases smoothly with energy consistent with the optical model, and that the rapid drop of $\sigma_{fus} \alpha 1/E_{c.m.}$ arises from the reduction of the evaporation residue cross section and a corresponding increase in σ_{DI}.

VI. CONCLUSION

The evaporation residue cross sections were measured for the $^{14}N + ^{10}B$ system up to a ^{14}N bombarding energy of 180 MeV. Energy spectra, angular distributions, and total yields of the evaporation

residues were compared with Hauser-Feshbach Monte Carlo calculations and the satisfactory agreement found suggests that, even at the highest energy, a statistically equilibrated compound nucleus is formed. The measured fusion cross sections are significantly smaller than the total reaction cross sections, and the difference between them increases with incident energy. Comparisons to fusion measurements of the $^{12}C + ^{12}C$ system demonstrate that the fusion of $^{14}N + ^{10}B$ is limited by the entrance channel alone; compound nucleus effects (i.e., a yrast line) are not the limiting factor for $^{10}B + ^{14}N$. This is a consequence of the large separation energy which inhibits the ability of the $^{14}N + ^{10}B$ fusion reaction to bring as much angular momentum into the compound nucleus as does $^{12}C + ^{12}C$ for a given excitation energy in ^{24}Mg.

Above center-of-mass energies of 60 MeV the $^{14}N + ^{10}B$ fusion cross section decreases proportionally to $1/E_{c.m.}$ indicating a saturation of J_c at about $J_c = 21 \pm 1$ h for this particular channel. This value of the maximum angular momentum is three units lower than that expected on the basis of rotating liquid drop limit calculations. The data available in the literature for the $^{12}C + ^{12}C$ system do not show an angular momentum saturation; more data are needed for these light systems at energies above 18 MeV/A to clarify this situation with regard to angular momentum saturation.

Oak Ridge National Laboratory is operated by Union Carbide Corporation for the U.S. Department of Energy under Contract No. W-7405-eng-26.

---

*On sabbatical leave from Instituto de Fisica, Universidad Nacional Autonomade de Mexico, Mexico.
†Present address: Lawrence Berkeley Laboratory, Berkeley, California 94720.
‡On leave from Commission Nacional de Energia Atomica, Buenos Aires, Argentina.

[1]B. Tamain, C. Ngo, J. Peter, and F. Hanappe, Nucl. Phys. A252, 187 (1975).
[2]R. G. Stokstad, in *Proceedings of the International Conference on Reactions Between Complex Nuclei, Nashville, Tennessee, 1974,* edited by R. L. Robinson, F. K. McGowan, J. B. Ball, and J. H. Hamilton (North-Holland, Amsterdam, 1974), Vol. II, p. 327.
[3]A. Weidinger, F. Busch, G. Gaul, W. Trautmann, and W. Zipper, Nucl. Phys. A263, 511 (1976).
[4]P. Sperr, T. H. Braid, Y. Eisen, D. G. Kovar, F. W. Prosser, Jr., J. P. Schiffer, S. L. Tabor, and S. Vigdor, Phys. Rev. Lett. 37, 321 (1976).
[5]M. Conjeaud, S. Gary, S. Harar, and J. P. Wieleczko, Nucl. Phys. A309, 515 (1978).
[6]D. Horn, A. J. Ferguson, and O. Hausser, Nucl. Phys. A311, 238 (1978).
[7]J. Gomez del Campo, R. A. Dayras, J. A. Biggerstaff, D. Shapira, A. H. Snell, P. H. Stelson, and R. G. Stokstad, Phys. Rev. Lett. 43, 26 (1979).
[8]F. Saint-Laurent, M. Conjeaud, S. Harar, J. M. Loiseaux, J. Menet, and J. B. Viano, Nucl. Phys. A327, 517 (1979).
[9]J. Gomez del Campo, R. G. Stokstad, J. A. Biggerstaff, R. A. Dayras, A. H. Snell, and P. H. Stelson, Phys. Rev. C 19, 2170 (1979).
[10]M. N. Namboodiri, E. T. Chulick, and J. B. Natowitz, Nucl. Phys. A263, 491 (1976).
[11]R. L. Parks, S. T. Thornton, L. C. Dennis, and K. R. Cordell, Nucl. Phys. A348, 350 (1980).
[12]R. G. Stokstad, D. C. Hensley, and A. H. Snell, Nucl. Instrum. Methods 141, 499 (1977).
[13]J. Gomez del Campo and R. G. Stokstad, Oak Ridge National Laboratory Technical Memo No. ORNL-TM-7295, 1981.
[14]C. K. Gelbke, M. Bini, C. Olmer, D. L. Hendrie, J. L. Laville, J. Mahoney, M. C. Mermaz, D. K. Scott, and H. H. Wieman, Phys. Lett. 71B, 83 (1977).
[15]R. Y. Cusson, J. Gomez del Campo, J. A. Maruhn, and V. Maruhn-Rezwani, Phys. Rev. C 23, 2524 (1981).
[16]W. D. Rae, R. G. Stokstad, B. G. Harvey, A. Dacal, R. LeGrain, J. Mahoney, M. J. Murphy, and T. J. M. Symons, Phys. Rev. Lett. 45, 884 (1980).
[17]J. S. Blair, in *Lectures in Theoretical Physics,* edited by P. D. Kunz and W. E. Britten (University of Colorado, Boulder, 1966), Vol. VIIIC, p. 375.
[18]S. K. Penny (unpublished).
[19]S. Cohen, F. Plasil, and W. J. Swiatecki, Ann. Phys. (N.Y.) 82, 557 (1974).
[20]D. G. Kovar, D. F. Geesaman, T. H. Braid, Y. Eisen, W. Henning, T. R. Ophel, M. Paul, K. E. Rehn, S. J. Sanders, P. Sperr, J. P. Schiffer, S. L. Tabor, S. Vigdor, B. Zeidman, and F. W. Prosser, Jr., Phys. Rev. C 20, 1305 (1979).
[21]S. M. Lee, T. Matsuse, and A. Arima, Phys. Rev. Lett. 45, 165 (1980).
[22]R. Vandenbosch and J. Lazzarini, Phys. Rev. C 23, 1074 (1981).
[23]R. Vandenbosch, Phys. Lett. 87B, 183 (1979).